Aerosol and Air Quality Research, 15: 799–813, 2015

ISSN: 1680-8584 print / 2071-1409 online
doi: 10.4209/aaqr.2014.09.0190

Mode and Place of Origin of Carbonaceous Aerosols Transported From East Asia to Cape Hedo, Okinawa, Japan

Kojiro Shimada[1,2*], Masamichi Shimada[1], Akinori Takami[3], Shuichi Hasegawa[4], Akihiro Fushimi[3], Takemitsu Arakaki[5], Watanabe Izumi[1], Shiro Hatakeyama[1]

[1] *Graduate School of Agriculture, Tokyo University of Agriculture and Technology, 3-5-8 Saiwaicho, Fuchu, Tokyo 183-8509, Japan*
[2] *Tokyo Metropolitan Research Institute for Environmental Protection, 1-7-5 Shinsuna, Kouto, Tokyo 136-0075, Japan*
[3] *National Institute for Environmental Studies, 16-2 Onogawa, Tsukuba, Ibaraki 305-8506, Japan*
[4] *Center for Environmental Science in Saitama, 914 Kamitanadare, Kazo, Saitama 347-0115, Japan*
[5] *University of the Ryukyus, 1 Senbaru, Nishihara-cho, Okinawa 903-0213, Japan*

ABSTRACT

This study investigated the source categories and emission areas of carbonaceous aerosols transported from East Asia to the East China Sea. Mass concentrations of heavy metals, ionic components, organic carbon, and elemental carbon (EC) were measured at the Cape Hedo Atmosphere and Aerosol Monitoring Station in Okinawa, Japan, throughout 2010. The relative influences of different categories of aerosols were determined by positive matrix factorization, and the source regions of each emissions category were evaluated by using the total potential source contribution function. Five source categories were identified: dust, sea salt and nitrate, secondary species, coal combustion, and oil combustion. The results showed that the major source of aerosols in North China is coal combustion, whereas the major source in South China, Japan, and Korea is oil combustion. The relative contributions of the five sources to EC concentrations at Cape Hedo were dust 7.0%, sea salt and nitrate 19.1%, secondary species 28.5%, oil combustion 12.8%, and coal combustion 32.6%. In particular, wintertime coal combustion in residential areas of North China contributed significantly to EC in 2010. The results also indicate that the contribution of coal combustion in source areas was higher in winter (52%), whereas the contribution of oil combustion was higher in spring (33%).

Keywords: Carbonaceous aerosols; Source area; Emission area; Contribution to EC.

INTRODUCTION

Elemental carbon (EC), also known as black carbon, originates from incomplete combustion of fuel during anthropogenic activities such as fossil fuel combustion, biomass burning, and biofuel burning for cooking and heating. EC has attracted attention recently, not only because it is now considered to be the second largest contributor to global warming but also because the effects of light-absorbing climate forcing agents depend on their source. reported As Ramana *et al.* (2010) reported: Fossil-fuel-dominated black-carbon plumes were approximately 100% more efficient warming agents than biomass-burning-dominated plumes. Numerous studies have reported similar findings (e.g., Ramanathan *et al.*, 2002; Hansen *et al.*, 2005; Novakov *et al.*, 2005; Kondo *et al.*, 2006; Han *et al.*, 2009; Xu *et al.*, 2009; Jacobson, 2010; Jeong *et al.*, 2011; Koch *et al.*, 2011; UNEP and WMO, 2011; Oshima *et al.*, 2012; Bond *et al.*, 2013).

There are large uncertainties in estimates of the global and regional effects on climate of combustion emissions because of a lack of long-term global and regional monitoring of aerosol composition, especially of aged and regionally dispersed aerosols.

At present in Asia, under the auspices of the Atmospheric Brown Cloud (ABC) project of the United Nations Environment Programme (UNEP), ABC observatories have been established to investigate the long-term effects of aerosols on climate in East Asia and South Asia (Lee *et al.*, 2007; Miyazaki *et al.*, 2007; Ramanathan *et al.*, 2007; Stone *et al.*, 2007). Observations by the Cheju ABC Plume Monsoon Experiment made during summer 2008 have been used to determine the dependence of the warming (or cooling) effect of ABCs on the source of the black carbon (Flowers *et al.*, 2010; Ramana *et al.*, 2010). Thus, aerosols transported from East Asia to the East China Sea are known

* Corresponding author.
Tel.: +81-42-367-5620
E-mail address: shimada-k@tokyokankyo

to have an important influence on the regional atmospheric environment.

At the Cape Hedo Atmosphere and Aerosol Monitoring Station (CHAAMS) in Okinawa, Japan, a major UNEP-ABC project site (Nakajima *et al.*, 2007; Takami *et al.*, 2007), we have been observing air pollutants to understand climate change and health hazards since 2006. In analyses of these data, we have focused on the inorganic components of secondary species, such as sulfates and nitrates, as well as on carbonaceous aerosols, including organic carbon (OC), EC, and polycyclic aromatic hydrocarbons.

This study is part of the Impacts of Aerosols in East Asia on Plants and Human Health project, which has as one of its objectives the determination of seasonal variations of heavy metals in aerosols collected at CHAAMS to provide basic data for research on the effects on human health of aerosols transported over long distances (Hatakeyama *et al.*, 2014). EC carries polycyclic aromatic hydrocarbons and heavy metals, which are harmful to human health (Gelencser, 2004). In this study, we analyzed data on pollutants collected at CHAAMS by using positive matrix factorization (PMF) to identify the relative contributions to EC of various source categories in the observed data. We then used the potential source contribution function (PSCF) to identify the regions from which EC of those categories was emitted.

METHODS

Observations

CHAAMS (26.87°N, 128.25°E; 60 m above sea level) is at the northern end of Okinawa Island, about 100 km from Naha, the largest city on the island, and about 650 km from Shanghai, a major city on the Chinese mainland. There are no large industrial or residential areas near CHAAMS. Air masses reaching CHAAMS are transported from China, Korea, Japan, Southeast Asia, or the Pacific Ocean, depending on seasonal wind patterns, so this site is suitably located to observe the long-range transport of air pollutants from East Asia.

We conducted intensive observation at CHAAMS throughout 2010. We collected a total of 45 daily samples during spring (25 March–15 April), summer (17–21 July), fall (23–26 October), and winter (6 December–12 January).

Aerosol particles for analyses of heavy metals and ionic components were collected on a Teflon filter (20.32 cm × 20.54 cm, Poreflon wp-500-50, Sumitomo Electric, Osaka, Japan) using a high-volume air sampler (Sibata, HV-1000F, Tokyo, Japan). A $PM_{2.5}$ impactor (Kaneyasu, 2010) was used in our high-volume air sampler, which was operated at a flow rate of 750 L/min. Sampling duration was 24 h.

Heavy metal species were analyzed with an inductively coupled plasma mass spectrometer (Agilent7500, Santa Clara, California, USA). Teflon filters were digested in a solution of nitric and hydrofluoric acid in a Teflon vessel during microwave radiation. Forty-eight trace metal species were analyzed (Hatakeyama *et al.*, 2011).

For analyses of ionic composition, filter samples were ultrasonically extracted with distilled water (specific resistivity > 18 mol/L·cm) and then analyzed for major ionic species by ion chromatography (C-R6A, Shimazu, Kyoto, Japan) (Hatakeyama *et al.*, 2011). Anion species (Cl^-, NO_3^-, and SO_4^{2-}) were analyzed in an A4 separation column, and cation species (Na^+, NH_4^+, K^+, Mg^{2+}, and Ca^{2+}) were analyzed in a CS12A separation column. The eluent was 1.8 mol/L Na_2CO_3/1.7 mmol/L $NaHCO_3$ for anions, and 18 mmol/L methanesulfonic acid for cations. The detection limits of heavy metal species and the ionic compositions have been reported by Hidemori *et al.* (2014).

Aerosol particles for analyses of OC and EC in $PM_{2.5}$ were collected on quartz microfiber filters with a diameter of 47 mm (2500QAT-UP, Pallflex 2500QAT-UP, Pall, East Hills, New York, USA) with an FRM 2025 apparatus (Thermo Electron Corporation, Franklin, Massachusetts, USA) operated at a flow rate of 16.7 L/min. None of the quartz fiber filters were baked before sampling because the amount of volatile organic compounds adsorbed onto unbaked quartz fiber filters is lower than the amount adsorbed onto baked quartz fiber filters (900°C) (Hasegawa, 2014). Three categories of blank filters were used: field (4 filters per month), travel (6 filters per month), and laboratory (4 filters per month). A 0.5 m^2 filter punch was analyzed for OC and EC using a Desert Research Institute (DRI) Model 2001 thermal/optical carbon analyzer (DRI, Reno, Nevada, USA) for eight carbon fractions following the Interagency Monitoring of Protected Visual Environments thermal/optical reflectance protocol (Chow *et al.*, 2001). The detection limits of OC and EC were 0.90 and 0.10 μg/m^2, respectively.

OC and EC in $PM_{2.5}$ were collected daily on quartz microfiber filters only during March and April 2010. However, OC and EC concentrations in aerosols were also continuously measured by an ambient carbon particulate monitor (Model 5400, Rupprecht & Patashnick Co. Inc., Albany, New York, USA) at 3-h intervals since 2004. Ambient aerosols of diameter > 2.5 μm were excluded by using a $PM_{2.5}$ cyclone with a 50% cutoff efficiency for 2.5 μm particles, and the < 2.5 μm fraction was collected on an impactor with a 50% effective cutoff diameter of 0.14 μm at a flow rate of 16.7 L/min. A 28.8-mm internal diameter straight pipe (about 3.5 m long) was used.

The thermal/optical method (DRI instrument) provides more accurate results than the thermal method (Model 5400 ambient carbon particulate monitor) because the trapping efficiency of the instrument is greater. Thus, if we assume that the data obtained by DRI are correct, in order to use the intensive observation data obtained by the Model 5400 monitor, we need to correct that data. According to Quincey *et al.* (2009) and Green *et al.* (2007), a correction coefficient can be determined by calculating the ratio of the results obtained by the thermal/optical method to those obtained by the thermal method. We calculated correction coefficients by using the daily measured raw data from the DRI instrument and the data from the Model 5400 instrument obtained from March to May in 2010 and 2011.

$$EC = (1.5 \pm 0.23)\ EC_{5400} + (0.16 \pm 0.034),$$
$$OC = (2.3 \pm 0.23)\ OC_{5400} + (0.11 \pm 0.10), \quad (1)$$

where EC_{5400} and OC_{5400} represent the EC and OC data

obtained with the Model 5400 monitor. Details of the calculation of the correction coefficients will be reported elsewhere.

The filters were analyzed gravimetrically for $PM_{2.5}$ mass concentrations by using a Sartorius MC5 electronic microbalance (Sartorius, Gottingen, Germany; sensitivity ± 1 μg) after equilibration for 24 h at 25°C at a relative humidity of 50% in an air-conditioned chamber (CHAM-1000, HORIBA, Kyoto, Japan).

Positive Matrix Factorization

PMF is a statistical analysis method that uses error estimates to produce non-negative results (Paatero and Tapper, 1994). We used the three-dimensional PMF program version 3.0 of the US Environmental Protection Agency (Norris, 2008). In this study, to identify the source categories by PMF analysis, we first determined 1) the optimal number of factors; 2) the stability and uncertainty of the solution; and 3) the rotation space (Norris, 2008). Thus, we evaluated the results of 1) base runs, 2) a bootstrap run, and 3) an F matrix. Table S1 summarizes the chemical components used in the PMF processing. Some metallic components of anthropogenic origin that were below the detection limit, particularly in summer, were considered to be missing (see seasonal variations in Results and Discussion). For each of these components, half the value of the detection limit was used, and their estimated errors were evaluated as 5/6 of the detection limit (Norris *et al.*, 2008). Then, the signal-to-noise (S/N) ratio of all data was examined to ascertain whether the measurement variability was real or within the noise level (Norris *et al.*, 2008), where species with S/N ratios greater than 2 are considered strong. In our data, all S/N ratios were greater than 2 so we classified all of the chemical components as strong species. We also plotted the predicted concentrations in base runs against the observed concentrations to confirm the validity of the calculations. The model results for most of the selected species were good (Table S1).

To determine the optimal number of factors, it is necessary to test different numbers of factors and then evaluate the PMF calculation results (Bhanuprasad *et al.*, 2008; Kitayama *et al.*, 2010). We carried out 20 random runs and retained the runs that produced minimum Q values for three to ten factors in base runs. Minimum Q decreases as the number of factors increases. In our results the slope of the relationship began to level off at five factors, with only small decreases for each additional factor beyond five (Fig. S1(a)). Both the maximum individual column mean, IM, and the maximum individual column standard deviation, IS, of the scaled residual matrix decreased sharply for solutions with five or more factors (Fig. S1(b)). Therefore, we adopted a five-factor solution.

To obtain reliable PMF results, it is desirable to utilize as many samples as possible. However, previous studies have used as few as 25 to 30 samples for PMF analyses (Bhanuprasad *et al.*, 2008; Mehta *et al.*, 2009; Cherian *et al.*, 2010). To estimate stability and uncertainty in factor contributions, we performed a bootstrap model analysis and analyzed the estimated contributions of the five factors. We evaluated the uncertainties by examining the contributions and concentrations of the five factors (Figs. S2 and S3). We found that the interquartile range (uncertainty) of key species was around 20% or smaller. Bhanuprasad *et al.* (2008), Mehta *et al.* (2009), and Cherian *et al.* (2010) reported an estimated uncertainty in the contribution of each factor of <~15%. Moreover, Norris *et al.* (2008) also evaluated the estimated uncertainty in the contribution of each factor to be around 30%. An uncertainty of 20% was acceptable given the results reported by these studies.

The uncertainties of the discrete difference percentiles of the key species in the five factors were within the 99% confidence interval of each concentration.

Fpeak values of −1.0 to +1.0 were used with the base runs. We applied to +1.0 with the based runs in this study. However, the trend of most contributions did not change noticeably in relation to the base run result.

Potential Source Contribution Function

We performed a PSCF analysis (Hopke *et al.*, 1995; Pekney *et al.*, 2006; Cherian *et al.*, 2010) to identify the preferred atmospheric transport pathways from sources to receptors for the source categories identified by the PMF analyses (PMF-PSCF). To investigate the transport pattern, we first calculated back trajectories (NOAA ARL HYSPLIT4; Draxler and Rolph, 2003) with data starting at 500 m altitude. Significant downward mixing of air masses from different arrival heights was evident at receptor locations, indicating a contribution from elevated transport to measured ground-level concentrations (Hopke *et al.*, 1995). This result led us to use PSCF (described below) to estimate the back trajectories at arrival heights of 500, 1000, and 1500 m. Four-day back trajectories at 2-h intervals were computed for arrival heights of 500, 1000, and 1500 m for each of the 45 daily mean samples.

PSCF estimates the conditional probability function that describes the spatial distributions of the probable source locations that contributed the pollutants observed during a given time period. The source domain is divided into a number of grid cells at a specific resolution, typically 1° × 1° (Kim and Hopke, 2004). The PSCF is defined as

$$PSCF_{ij} = \frac{P[B_{ij}]}{P[A_{ij}]} = \frac{m_{ij}/N}{n_{ij}/N} = \frac{m_{ij}}{n_{ij}}, \quad (2)$$

where n_{ij} is the number of all points in the ij^{th} cell; here, the number of points is usually equal to the number of back trajectories passing through the ij^{th} cell, but it is defined as the number of "end-points" calculated by back trajectory analyses. End-points are defined as the locations of the air mass calculated by back trajectory analyses at every hour from the start time of the trajectory. $P[A_{ij}]$is the probability given by n_{ij}/N; N is the total number of points summarized over all cells in the modeling region; m_{ij} is the number of points in the ij^{th} cell that are classified as having a PMF factor exceeding the threshold value (> 50%); and $P(B_{ij})$ is the probability given by m_{ij}/N. These conditional probabilities

are computed for different pressure levels. Hence, the total probability of material transfer from various heights is calculated from the conditional probabilities associated with each height (Hopke *et al.*, 1995). We used the following weighting function:

$$W\left(n_{ij}\right)=\begin{cases}1.0 & 75<n_{ij}\\ 0.7 & 25<n_{ij}\le 75\\ 0.4 & 8<n_{ij}\le 25\\ 0.2 & n_{ij}\le 8\end{cases}. \quad (3)$$

For the PSCF calculation, the source domain was restricted to latitudes 20°N–55°N and longitudes 90°E–150°E to suppress erroneous identification of distant PSCF regions with negligible mean residence times of air masses (Hopke *et al.*, 1995). Regions with PSCF values ranging from 0.5 to 1 were designated as probable source regions for each factor during the study period.

RESULTS AND DISCUSSION

Seasonal VARIATIONS

Seasonal mass concentrations at CHAAMS of metallic and ionic species, OC, and EC, and the aerosol mass concentration in $PM_{2.5}$ during 2010 are presented in Fig. 1. These chemical components were all high during spring and winter but low during summer at CHAAMS. Those in $PM_{2.5}$, however, were all high during spring and winter but low during summer at CHAAMS. Approximately 80% of the total air masses in spring and winter were transported from China to CHAAMS, as indicated by back trajectory analysis (Shimada *et al.*, 2011). Therefore, air pollutants were transported from the Asian continent during spring and winter. Table 1 shows seasonal average concentrations of anthropogenically derived and naturally occurring trace-element and metallic species (Al, Mn, Ba, Sr, Fe, Mg, V, Zn, Ni, Cu, As, Se, Cd, and Pb). Average concentrations of potentially toxic heavy metals from anthropogenic sources (V, Ni, Zn, As, Se, Cd, Pb, and Cu) were highest in spring (Table 1 and Fig. 1(a)). The average concentration in $PM_{2.5}$ of Al, which is a major component of soil, was highest during summer. This result suggests that some local dust was transported to CHAAMS in summer.

Table 2 shows seasonal mass concentrations of major ions (Na^+, K^+, NH_4^+, Mg^{2+}, SO_4^{2-}, NO_3^-, Cl^-, and Ca^{2+}), $PM_{2.5}$, OC, and EC. Ion balances were acidic in winter and spring and alkaline in summer and autumn. The acidity of $PM_{2.5}$ was controlled mainly by sulfate (Fig. 1(b)).

The seasonal variations we obtained agree with the findings of Takiguchi *et al.* (2008) and Shimada *et al.* (2011), who reported high concentrations of nitrate, $PM_{2.5}$, OC, EC, CO, O_3, and major ionic components in rainwater during spring and winter and low concentrations during summer at CHAAMS. These investigators interpreted these data to indicate that pollutants, including acidic species and toxic metals in $PM_{2.5}$, are transported to CHAAMS by migratory high-pressure systems and cold fronts from the Asian continent during spring and winter. The data also suggest that southerly monsoon winds transported clean oceanic air masses to CHAAMS from the Pacific Ocean during summer. OC, EC, and aerosol mass concentrations of $PM_{2.5}$ ranged from 0.04 to 1.69 μgC/m^3 (OC), 0.03 to 0.68 μgC/m^3 (EC), and 0.03 to 29 μg/m^3 ($PM_{2.5}$) (Table 2 and Fig. 1(c)). These concentration ranges of OC and EC are comparable to those observed at Gan and Hanimaadhoo in India (Stone *et al.*, 2007).

The levels of EC that we observed are well above the levels expected in rural locations, but they are considerably lower than those observed in urban settings on the Asian continent (Lin and Tai, 2001; Feng *et al.*, 2006; Zhang *et al.*, 2008). Although the K^+ concentration can be used as an indicator of biomass burning, the concentration is lower in our data from CHAAMS than the concentrations reported at Gan and Hanimaadhoo (Stone *et al.*, 2007). Biomass fuels are the main source of EC in South Asia (Gustafsson *et al.*, 2009), but not in East Asia (Stone *et al.*, 2007).

Identification of Source Categories of Aerosols Transported to Cape Hedo from the Asian Continent

On the basis of our PMF analysis results for specific inorganic elements and trace metals (Fig. 2), we identified the following five source categories of aerosols: dust (DUT), sea salt and nitrate (SSN), secondary species (SEP), oil combustion (OIC), and coal combustion (COC). Among these, DUT showed a high loading of crustal elements (Al, 78%; Fe, 55%) (Fig. 2(a)). NO_3^- has been reported to be associated with dust containing Ca^{2+} and sea salt (Laskin *et al.*, 2005; Takiguchi *et al.*, 2008), and Takiguchi *et al.* (2008) have reported that volatilized HNO_3 is taken up by coarse particles, such as dust particles, and that the reaction $CaCO_3 + 2HNO_3 \rightarrow Ca(NO_3)_2 + H_2O + CO_2$ produces particulate NO_3^-. Our PMF analysis did not identify NO_3^- as a major constituent of DUT, probably because we did not observe large amounts of Asian dust accompanying air pollution during our observation period. The crustal enrichment factor (EF), which is defined as

$$EF = ([Z]_{aerosol}/[Fe]_{aerosol})/([Z]_{crust*}/[Fe]_{crust*}), \quad (4)$$

where Z is the target element, has commonly been used to evaluate the strength of crustal versus noncrustal (i.e., anthropogenic) sources. EF < 2 suggests mainly natural crustal sources, and EF > 10 suggests strong enrichment from noncrustal sources (Gao *et al.*, 2002). The EF values in overall period (Al, 1.04; Mn, 1.68; Ba, 0.87; and Sr, 1.66) were very low and suggest natural sources. On the other hand, according to Lei *et al.* (2011) and Zhu *et al.* (2004), Ca and Mg in particulate matter in China are emitted by coal burning and by raw materials used in industrial processes, and these emissions have been increasing since 1990 (Lei *et al.*, 2011). Zhu *et al.* (2004) investigated the mass percentages of Ca and Mg in fly ash from coal combustion and in the raw materials used by non-metallic-mineral product industries in China. China's anthropogenic emissions of Ca and Mg might be larger than natural sources, although significant emissions of mineral dusts come with sand storms (Zhu *et al.*, 2004). In overall period,

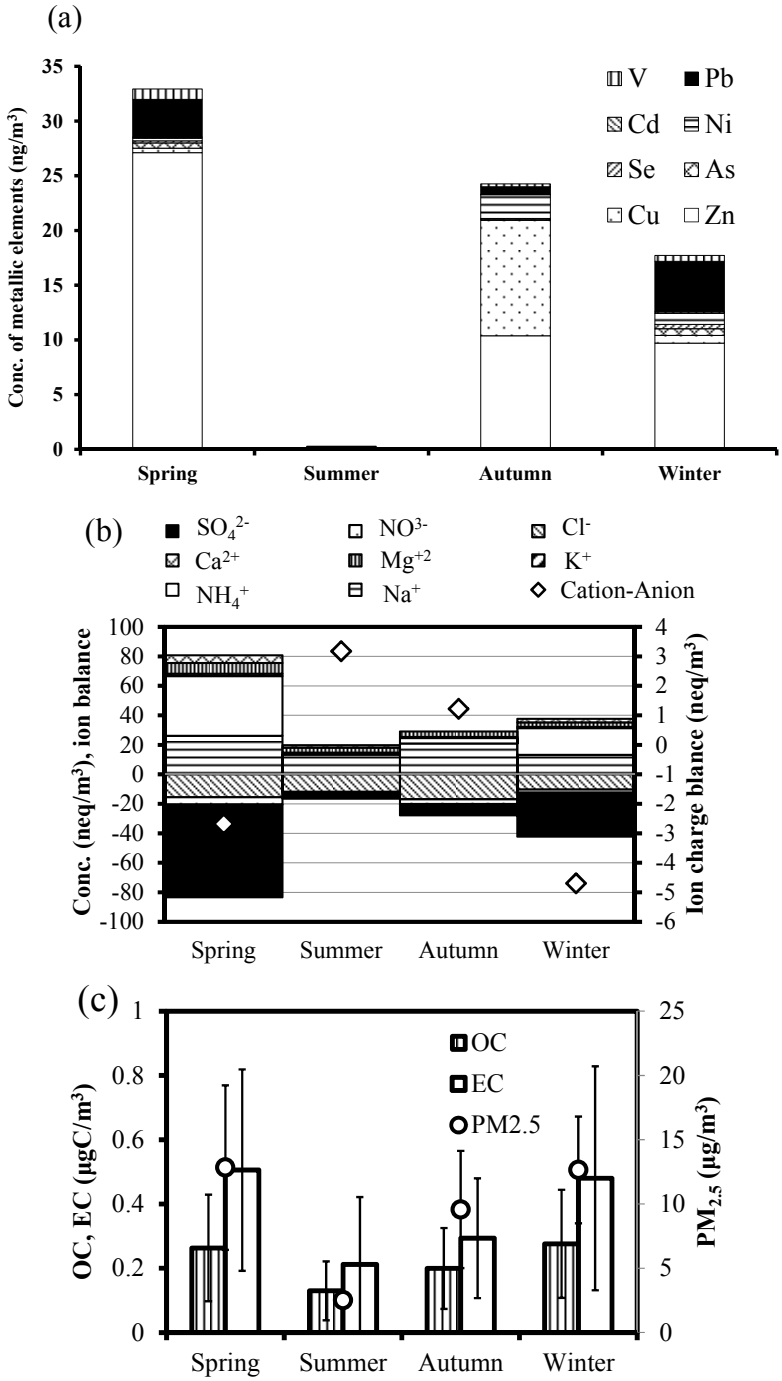

Fig. 1. Seasonal variation of (a) metallic element concentrations, (b) ionic species, and (c) OC, EC, and $PM_{2.5}$ mass concentrations measured at CHAAMS in 2010. In panel (b), the positive and negative concentrations are those of cations and anions, respectively, and the diamonds indicate net ion charge balances. In panel (c), error bars mean one standard deviation.

the EFs of Ca and Mg were also very low, 1.49 and 5.57, respectively. DUT did not contain NO_3^- (Fig. 2(a)); hence, DUT is not included among pollutants.

SSN showed the following loadings in our data: (NO_3^-, 42%; Na^+, 64%; and Cl^-, 80%) (Fig. 2(b)). Takiguchi *et al.* (2008) reported that volatilized HNO_3 is taken up by coarse particles such as sea salt by the reaction $NaCl + HNO_3 \rightarrow NaNO_3 + HCl$, yielding particulate NO_3^-; this reaction is known as the chlorine-loss reaction. According to Arakaki *et al.* (2006), chlorine loss commonly also occurs as a result of reactions with H_2SO_4 during Asian dust events containing air pollutants. Thus, both HNO_3 and H_2SO_4 can cause chlorine loss in aerosols. The main pollutant in SSN is NO_3^-.

SEP, which represents secondary SO_4^{2-} formation on primary combustion particles, showed high loadings of the compounds NH_4^+ (64%), SO_4^{2-} (56%), OC (15%), and EC (34%) (Fig. 2(c)). NH_4^+, SO_4^{2-}, and OC are tracer species.

Table 1. Seasonal mass concentrations of metallic species in $PM_{2.5}$ at CHAAMS in 2010. (N = number of samples, N.D. = Not Detected).

Season	Ni	Cu	Zn	As	Se	Cd	Pb
	ng/m^3	ng/m^3	ng/m^3	ng/m^3	ng/m^3	ng/m^3	ng/m^3
Spring	0.25 ± 0.32	0.40 ± 0.48	27 ± 32	0.488 ± 0.408	0.188 ± 0.260	0.091 ± 0.083	3.46 ± 3.38
Summer	N.D.	N.D.	N.D.	0.002 ± 0.002	N.D.	N.D.	0.21 ± 0.31
Autumn	2.17 ± 2.95	10.54 ± 10.58	10 ± 18	0.122 ± 0.085	0.057 ± 0.059	0.006 ± 0.010	0.72 ± 0.05
Winter	1.01 ± 1.76	0.70 ± 1.10	10 ± 12	0.618 ± 0.662	0.384 ± 0.412	0.137 ± 0.147	4.63 ± 5.57
Whole period	0.63 ± 1.47	1.35 ± 3.2	17 ± 26	0.442 ± 0.509	0.216 ± 0.320	0.088 ± 0.111	3.22 ± 4.18

Season	V	Mg	Al	Fe	Mn	Ba	Sr
	ng/m^3	ng/m^3	ng/m^3	ng/m^3	ng/m^3	ng/m^3	ng/m^3
Spring	0.95 ± 0.52	88 ± 52	119 ± 96	63 ± 67	88 ± 52	0.98 ± 0.62	1.02 ± 0.909
Summer	0.09 ± 0.03	32 ± 10	174 ± 98	N.D.	32 ± 10	0.37 ± 0.13	0.26 ± 0.03
Autumn	0.26 ± 0.12	61 ± 36	26 ± 10	19 ± 18	61 ± 36	0.34 ± 0.00	0.26 ± 0.06
Winter	0.55 ± 0.36	68 ± 32	103 ± 70	51 ± 46	68 ± 32	0.64 ± 0.33	0.81 ± 0.71
Whole period	0.67 ± 0.52	112 ± 91	112 ± 91	49 ± 58	71 ± 45	0.77 ± 0.55	0.79 ± 0.81

Table 2. Seasonal mass concentrations of $PM_{2.5}$, OC, EC, and ionic species at CHAAMS in 2010 (N = number of samples).

Season	Cl^-	NO_3^-	SO_4^{2-}	Na^+	NH_4^+	K^+	Mg^{2+}
	neq/m^3 (N = 45)	neq/m^3 (N = 45)	neq/m^3 (N = 45)	neq/m^3 (N = 45)	neq/m^3 (N = 45)	neq/m^3 (N = 45)	neq/m^3 (N = 45)
Spring	15.7 ± 10.2	4.8 ± 3.8	62.9 ± 38.6	26.1 ± 15.2	40.5 ± 26.1	1.5 ± 1.4	7.3 ± 4.3
Summer	11.9 ± 6	1 ± 0.4	3.6 ± 1.7	13.3 ± 6.6	0.8 ± 0.4	0.7 ± 0.2	3.3 ± 3
Autumn	17 ± 15.3	3.1 ± 2	7.7 ± 7.8	20.9 ± 17.1	3.7 ± 3.6	0.7 ± 0.6	3.7 ± 4.2
Winter	10.4 ± 13	1.9 ± 1.4	29.9 ± 15.3	13.2 ± 9.3	18.1 ± 10	0.9 ± 0.8	3 ± 1.6
Overall average	13.7 ± 11.2	3.3 ± 3.2	41.1 ± 36.4	20.2 ± 14.1	25.9 ± 24.4	1.2 ± 1.1	5.2 ± 4

Season	Ca^{2+}	Anions	Cations	OC	EC	TC	$PM_{2.5}$
	neq/m^3 (N = 41)	Total average (neq/m^3)	Total average (neq/m^3)	μg/m^3 (N = 40)	μg/m^3 (N = 45)	μg/m^3 (N = 45)	μg/m^3 (N = 44)
Spring	5.1 ± 3.2	83.3 ± 44.9	80.7 ± 42.4	0.51 ± 0.31	0.26 ± 0.17	0.77 ± 0.45	12.8 ± 6.4
Summer	1.6 ± 0.7	16.5 ± 6.2	19.7 ± 6.8	0.22 ± 0.21	0.13 ± 0.09	0.34 ± 0.16	2.5 ± 0.4
Autumn	N.D.	27.8 ± 19.1	29 ± 19.6	0.29 ± 0.19	0.2 ± 0.13	0.49 ± 0.31	9.6 ± 4.6
Winter	2.4 ± 1.9	42.3 ± 18.6	37.6 ± 14.5	0.48 ± 0.35	0.28 ± 0.17	0.76 ± 0.51	12.7 ± 4.2
Overall average	3.4 ± 3	58.2 ± 42.4	55.9 ± 40	0.42 ± 0.26	0.24 ± 0.15	0.71 ± 0.46	11.1 ± 5.5

Many PMF source apportionment studies have reported a relationship between ammonium sulfate and substances of combustion origin, such as EC and heavy metals (e.g., Kim *et al.*, 2004; Kim and Hopke, 2004). SEP also contained As, Se, and V. As discussed below, these elements are also key markers of OIC and COC. Therefore, the precursors of SEP derive from the OIC and COC source categories.

OIC was characterized by high loadings of V (55%) (Fig. 2(d)), which is a marker for oil combustion (Okuda *et al.*, 2006). COC had high loadings of As (52%) and Se (48%) (Fig. 2(e)), both of which are markers for coal combustion (Okuda *et al.*, 2006; Stone *et al.*, 2007). Coal includes many trace elements that are also evident in COC (Fig. 2(e)).

Our PMF analysis did not identify a biomass burning factor. Although K^+ is considered a marker for biomass combustion, Xu *et al.* (2003) reported that it can also be associated with coal combustion, Stone *et al.* (2007) also reported minute emissions of K^+ from coal burning. Zhang *et al.* (2009) reported that observation-based studies of source apportionment in atmospheric aerosols have shown that fossil fuel combustion is the main source of EC in East Asia. However, we could not detect a hot spot in China for biomass burning in satellite imagery (MODIS; http://web modis.iis.u-tokyo.ac.jp/). Our results suggest that it might be difficult to identify a biomass burning factor at CHAAMS in spring and winter by using only K^+ as a marker for biomass combustion. However, Handa *et al.* (2010) reported that $^{14}C/^{12}C$ analysis of OC can be used to identify a biomass burning factor at CHAAMS in summer. Furthermore, Shimada *et al.* (2011) reported that OC/EC ratios and hot spots identified on MODIS images suggest that air pollution from biomass burning is transported to Cape Hedo from the Asian continent in June, although that transport was not clearly evident in the observed data of the present study. According to Yamaji *et al.* (2009) and Kanaya *et al.* (2008), the Mount Tai Experiment in 2006 indicated that agricultural waste burning had a considerable impact on summertime emissions in China, suggesting that the effect of biomass burning might be seasonal.

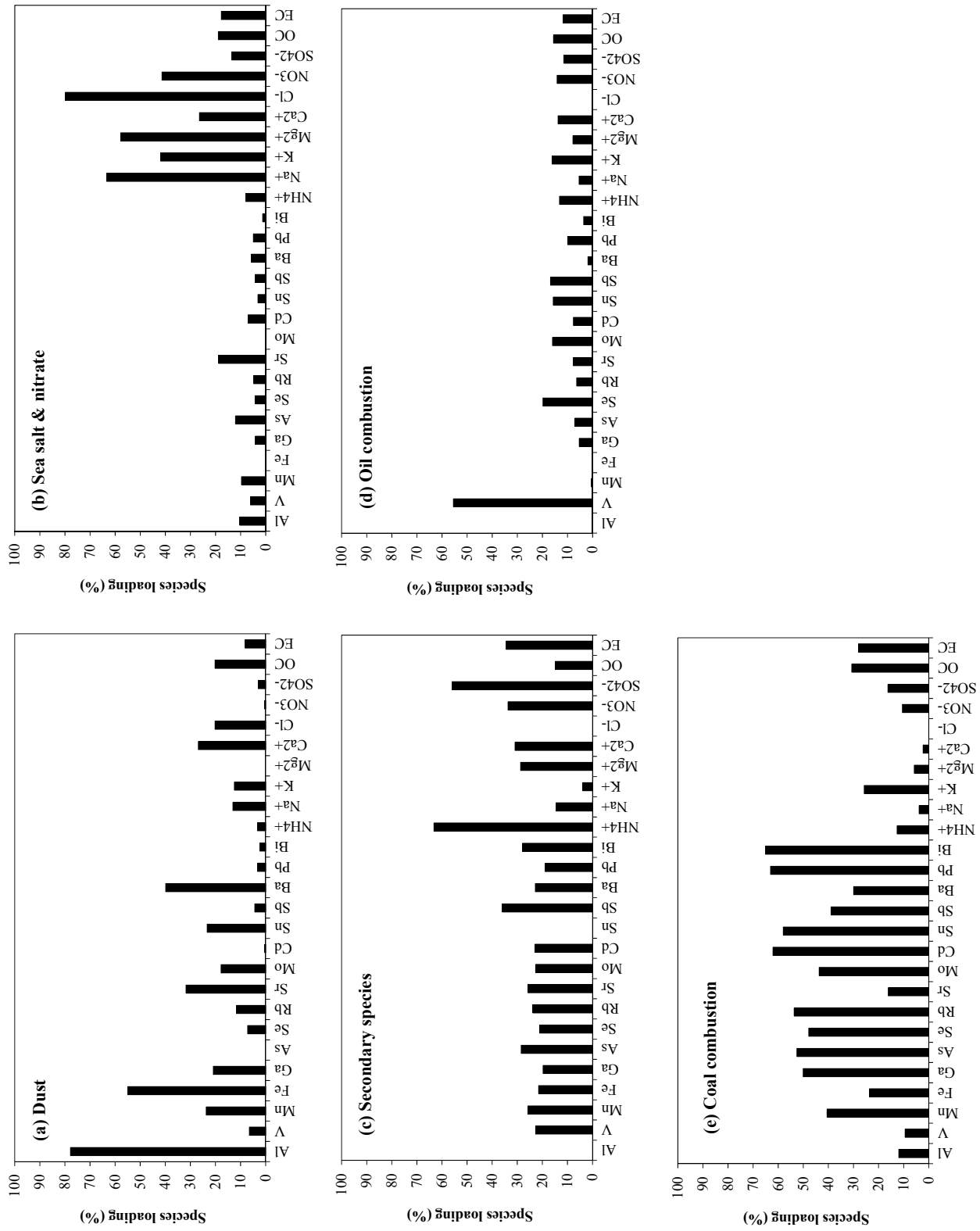

Fig. 2. PMF-predicted factor loadings on each source category in 2010: (a) dust, (b) sea salt and nitrate, (c) secondary species, (d) oil combustion, and (e) coal combustion.

Source Categories and Emission Regions from the PMF–PSCF Analysis Results

In this section we discuss the relative influences of natural and anthropogenic sources on aerosol loadings over East Asia on the basis of our PMF–PSCF analysis results (Fig. 3). The PMF-PSCF results provide information on the direction of air mass transport because the PSCF was based on back trajectory analysis results.

Dust and Sea Salt and Nitrate

Regions of North China and the Pacific Ocean contributed to DUT (Fig. 3(a)). In summer, the air mass over Cape Hedo monitoring station was a relatively clean Pacific Ocean air mass, and there were no significant emission sources nearby. Concentrations of the crustal elements Al and Fe in fine dust particles were high (Al, 112 ± 91 ng/m^3; Fe, 49 ±58 ng/m^3; mean ± standard deviation) during all of 2010 regardless of season (Table 1). This result suggests that some local dust emissions were included in the samples. The presence of DUT in potential source contributions from the oceanic area also is evidence of a soil source close to CHAAMS.

Many areas of both the Pacific Ocean and the East China Sea contributed to SSN (Fig. 3(b)), although there are no known strong sources of nitrate emissions in the Pacific Ocean. However, satellite observations have shown that ships are an important emission source of NO_x over the East China Sea (Richter *et al.*, 2004). NO_x is easily oxidized to HNO_3 by photochemical reactions in the atmosphere. During the transport of air pollutants to CHAAMS, gaseous

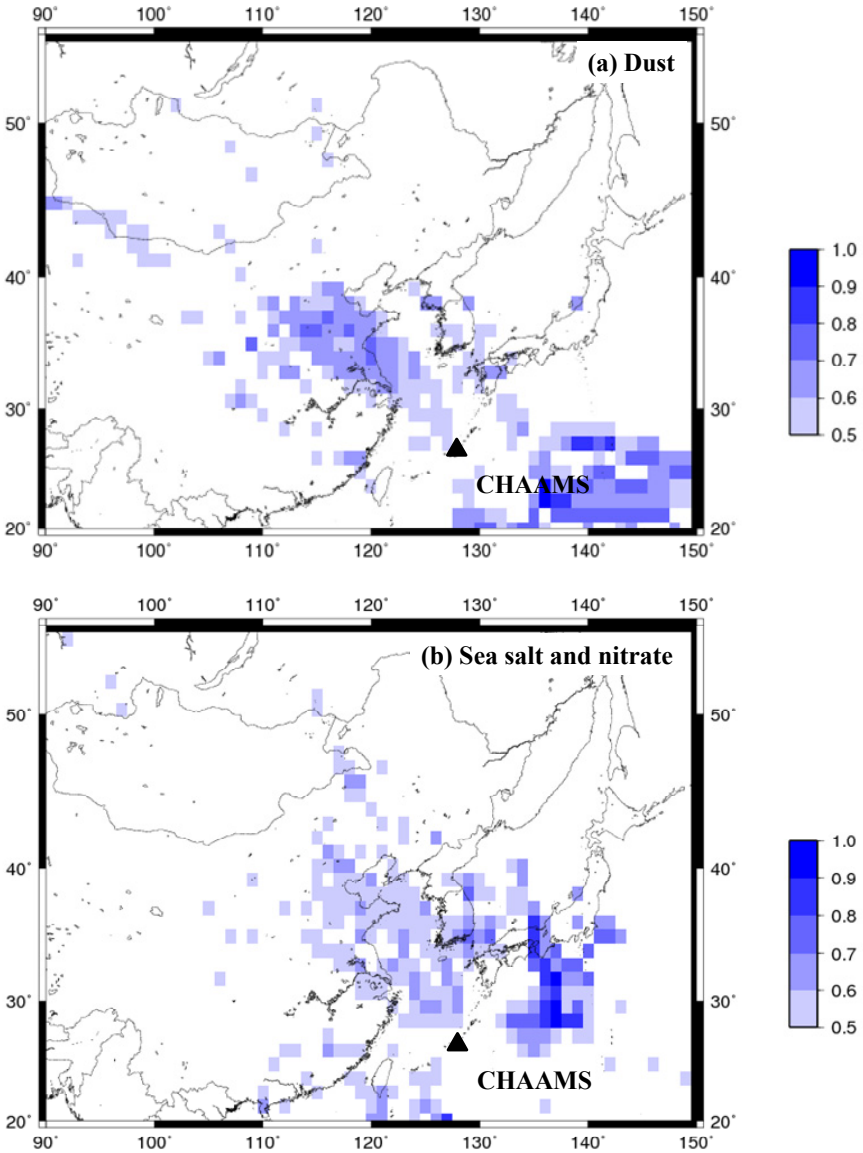

Fig. 3. Probable source regions based on the PMF–PSCF analysis of PMF-identified factors in 2010: (a) dust, (b) sea salt and nitrate, (c) secondary species, (d) oil combustion, and (e) coal combustion. PMF–PSCF values from 0.5 (50%) to 1.0 (100%), which we considered to indicate probable source regions, are shown for each factor. 0.5 value means the threshold value (50%) and and 1.0 value means maximum value in PMF factor. Closed triangle indicates a location of CHAAMS.

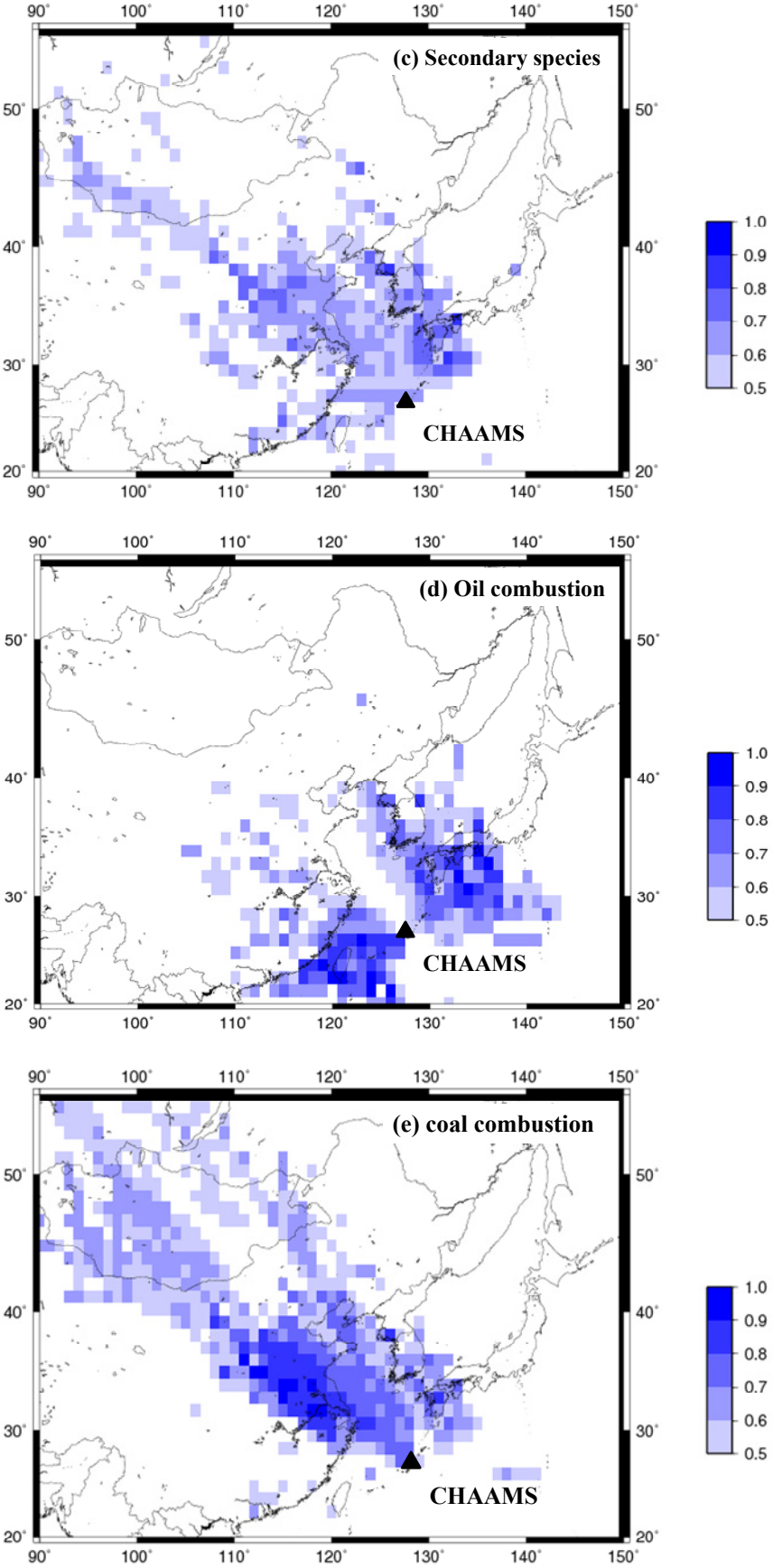

Fig. 3. *(continued).*

nitric acid reacts with sea salt to form nitrates by the reaction $HNO_3 + NaCl \rightarrow NaNO_3 + HCl$ (Takiguchi *et al.*, 2008).

Secondary Species

Areas of the East China Sea, the Korean Peninsula, and Japan contributed to SEP (Fig. 3(c)). The slope (0.75) of the correlation between NH_4^+ and SO_4^{2-} concentrations (Fig. 4) indicates that the contribution of SO_4^{2-} was high relative to that of NH_4^+, a result that agrees with the findings of Hatakeyama *et al.* (2006) and Takami *et al.* (2007). According to Hatakeyama *et al.* (2006), low NH_4^+/SO_4^{2-} molar ratios may indicate long transport distances or long residence times above the ocean, because NH_4^+ concentrations tend to decrease as a result of deposition, whereas those of SO_4^{2-} increase because of conversion of SO_2 to SO_4^{2-} during transport. According to Takami *et al.* (2007), when SO_4^{2-}/SO_y ($SO_y = SO_2 + SO_4^{2-}$) is high, NH_4^+/SO_4^{2-} is low. The same reasoning can be applied to explain the low ratio of organics to SO_4^{2-} in our results.

Cloud processing also has an important influence on the concentrations of the components of SEP. Efficient conversion of SO_2 to SO_4^{2-} during cloud processing can cause the SO_4^{2-}/SO_y ratio to be high even without aging of the air mass. Furthermore, NH_4^+ can be scrubbed from air masses by clouds. We interpreted the high SO_4^{2-} concentrations accompanied by low NH_4^+ concentrations during our observations to be the result of NH_4^+ deposition and cloud processing of chemical species during transport.

Oil and Coal Combustion

Areas contributing to OIC included Japan, the Korean Peninsula, and Taiwan and South China (Fig. 3(d)), whereas the main area contributing to COC was North China (Fig. 3(e)). In particular, the contributions from around Beijing and Xian to COC were high (Fig. 3(e)).

Ohara *et al.* (2007) and Zhang *et al.* (2009) reported that coal and oil consumption is increasing in China. The main contributors of coal combustion are coal-burning industrial facilities and residential areas. There are many coal-burning industrial facilities throughout China, but residential areas that burn bituminous raw coal are mainly in northern China. The increased oil combustion is due to increases in industrial facilities and, especially, the number of passenger cars. Regional differences of emissions are due mainly to spatial differences in economic development, industrial facilities, and population. Emissions from both oil and coal combustion are increasing mainly in eastern and central China. Oceanic areas near South China also contributed to OIC. This result suggests that a major source of OIC was ship emissions, a result consistent with satellite observations reported by Richter et al. (2004).

Using back trajectory analysis results, we classified the origins of the air masses that arrived at CHAAMS (Shimada *et al.*, 2011) into six areas (North China, South China, Korea, Japan, Pacific, and Southeast Asia). OC/EC ratios are useful for distinguishing the combustion of fossil fuels (low OC/EC) from biomass burning (high OC/EC). The OC/EC ratios in the air masses that originated in North and South China were 1.98 ± 0.05 and 2.83 ± 0.03, respectively, and the OC/EC ratios estimated for North and South China based on the Asian emission inventory data set range from 1 to 2 and from 2 to 3, respectively. Thus, our observational data are in accordance with the emissions inventory data. The low OC/EC ratios (< 3) in both North and South China indicate that the sources of EC and OC were anthropogenic, but we were not able to identify specific source categories for EC and OC in the air masses from North China, South China, Korea, and Japan (Shimada *et al.*, 2011).

Our maps clearly show characteristics of emission areas in China, and the maps are useful for evaluating and improving emissions inventory data.

Contributions of Different Source Categories to EC at CHAAMS

The relative contributions of the five source categories identified by PMF to ambient EC concentrations at CHAAMS in 2010 are presented in Fig. 5. The correlation between measured and predicted EC in overall period showed that the five identified factors reproduced well the measured masses of each category and reasonably accounted for the observed variations in EC. The contributions of each source category to EC were as follows: DUT, 7.0%; SSN, 19.1%; SEP, 28.5%; OIC, 12.8%; and COC, 32.6%. This result clearly showed the seasonal characteristics of emission areas in China.

The seasonal variations of the relative EC contributions

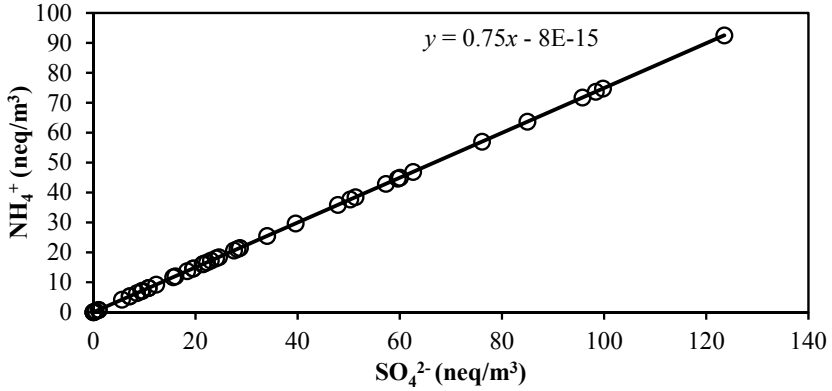

Fig. 4. Correlation between SO_4^{2-} and NH_4^+ concentrations calculated from the PMF analysis results.

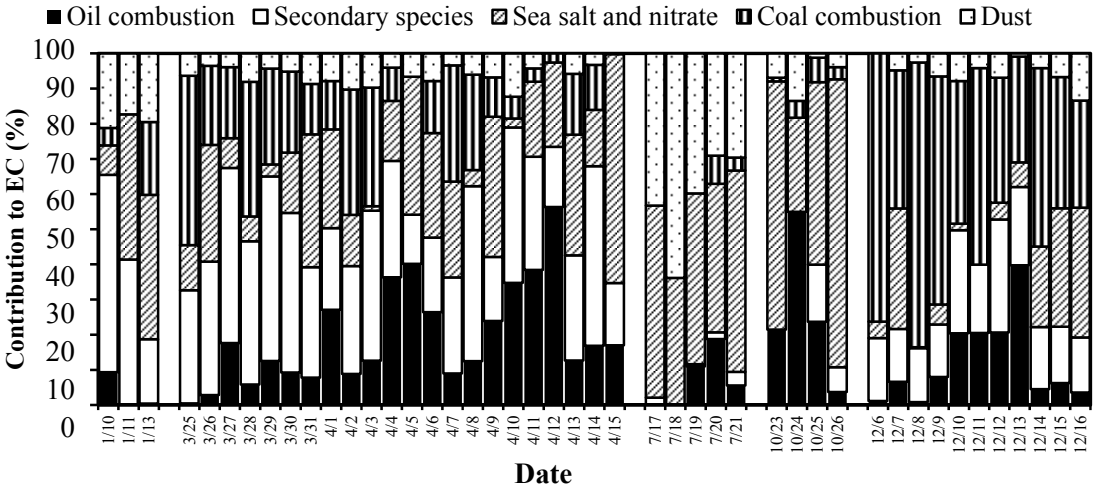

Fig. 5. Time series of the relative contributions of each of the five factors to EC in 2010, as calculated by the PMF model.

by the five factors (Fig. 5) suggest that EC is derived from both OIC and COC, and that the contribution of COC to EC is higher in winter than in other seasons. According to Lin *et al.* (2008), GOME (Global Model–Satellite) and CMAQ (Community Multi-scale Air Quality) model simulations have shown that the winter distribution of NO_x in North China is different from its distribution in other seasons, indicating that a particular but unidentified source contributes significantly to EC in North China during winter. Our results clearly showed that COC is the main source of EC in North China in winter (Fig. 3(e)). In particular, wintertime coal combustion in residential areas of North China contributed significantly to EC. Because the main COC source area is North China (Fig. 3(e)) and because COC is the main contributor to EC in winter, COC must be the main source of EC in North China in winter.

The contribution of COC to EC was highest in winter (52%), and that of OIC was highest in spring (33%) (Figs. 3(d), 3(e), and 5). On the basis of simultaneous observations at remote sites, Matsumoto *et al.* (2003) reported that the transport patterns of polluted air masses moving from East Asia to the northern Northwest Pacific are often different from those moving to the southern Northwest Pacific. In addition, the number of low- and high-pressure systems moving eastward from South China increases in spring (Uno *et al.*, 2000; Hatakeyama *et al.*, 2001; Shimada *et al.*, 2011). We observed both low- and high-pressure systems moving eastward from the Shanghai region of South China in spring. This seasonal difference in the contributions of different sources of EC in air pollution from North and South China can be identified in the observations at CHAAMS.

EC from SSN may be produced by ships powered by fossil fuels (Stone *et al.*, 2007). EC from SEP may reflect increases in the number of coated EC particles, because observations (Moteki *et al.*, 2007) and model studies (Oshima *et al.*, 2009) have shown that non-sea-salt sulfate and water-soluble OC can coat EC particles. Our results suggest that EC from SEP more actively provides cloud condensation nuclei than other source categories. The contribution of SEP to EC was higher in spring (34%) than in winter (24%) (Fig. 5), which is attributable to differences in light intensity and temperature between spring and winter; in particular, photochemical aging is enhanced in spring compared to winter.

The absolute contributions of each of the five factors to total EC at CHAAMS as calculated by the PMF model are presented in Fig. 6. Although the EC contribution from OIC was higher in spring than in other seasons (Fig. 5), the total contribution of OIC to EC was not high. In spring and winter, when the total EC concentration was high (Fig. 6), the contribution of COC to EC was higher than that of OIC. Shimada *et al.* (2011) reported that higher concentrations of EC are transported from North China than from South China, consistent with EC emission inventory data (Zhang *et al.*, 2009). Therefore, EC in transboundary air pollution was contributed in large part by coal combustion in China.

CONCLUSIONS

Carbonaceous aerosols and heavy metal concentrations measured at Cape Hedo, Okinawa, in 2010 showed that concentrations of both metallic elements and ionic components in aerosols were high during spring and winter but low during summer. From these results, we inferred that during spring and winter, atmospheric pollutants were transported from the Asian continent to CHAAMS by migratory high-pressure systems and cold fronts, whereas during summer, southerly monsoon winds transported clean oceanic air masses from the Pacific to CHAAMS. The observed OC, EC, and aerosol mass concentrations were comparable to concentrations measured at Gan and Hanimaadhoo, India, whereas the concentration of potassium was lower at CHAAMS than at Gan and Hanimaadhoo. This result suggests that much less EC is derived from the burning of biomass fuels in China compared with South Asia.

The relative contributions of source categories of aerosols were determined by PMF, and source regions of emissions were evaluated by using PSCF. Five source categories were identified: dust, sea salt and nitrate, secondary species, oil combustion, and coal combustion. Our results indicate that

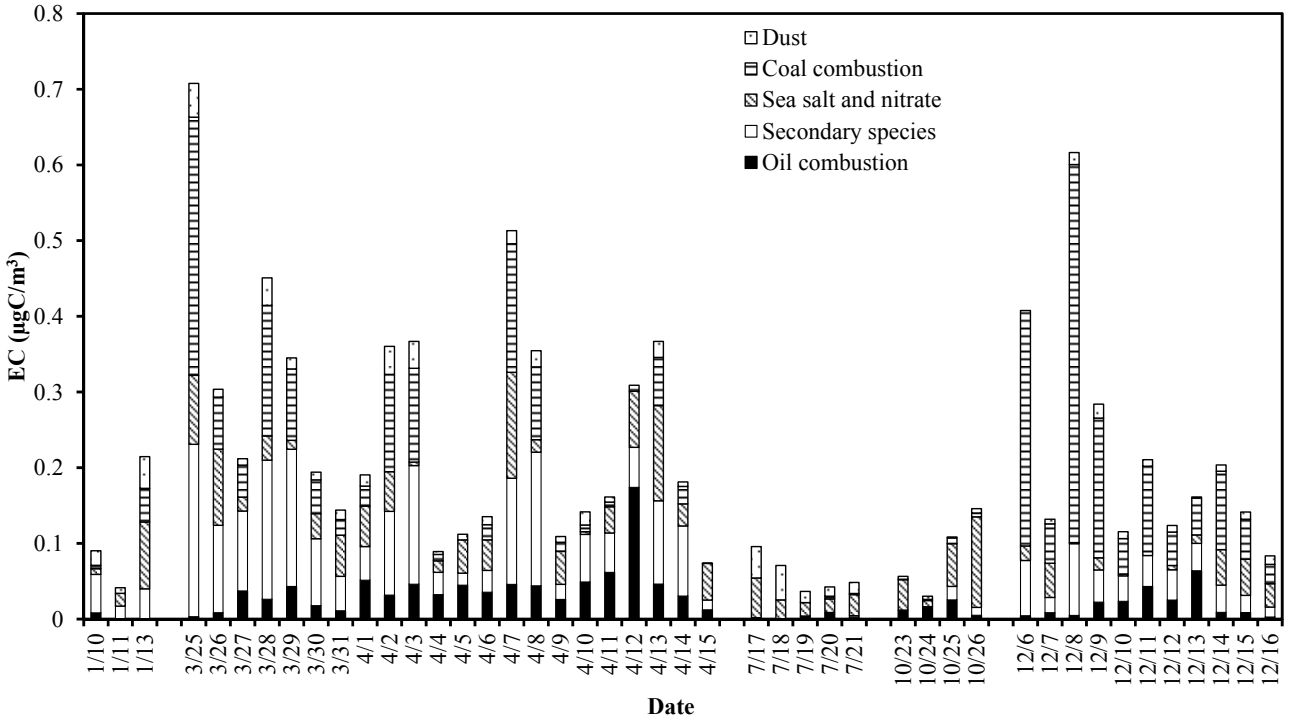

Fig. 6. Time series of the absolute contributions of each of the five factors to EC in 2010, as calculated by the PMF model.

there was a local soil source near CHAAMS that contributed dust, that the sea salt and nitrate contribution could be attributed to ships in the East China Sea, and that contributions from oil combustion in South China and from coal combustion in North China, were high.

The relative contributions of the five source categories to ambient EC concentrations at CHAAMS were as follows: dust, 7.0%; sea salt and nitrate, 19.1%; secondary species, 28.5%; oil combustion, 12.8%; and coal combustion, 32.6%. High contributions of secondary species were associated with the formation of cloud condensation nuclei. The contribution of coal combustion to EC was highest in winter, whereas that of oil combustion was highest in spring.

ACKNOWLEDGMENTS

This work was partly supported by Grant-in-Aid for Scientific Research on Innovative Areas No.4003 “Impacts of Aerosols in East Asia on Plants and Human Health” from the Ministry of Education, Culture, Sports, Science and Technology (MEXT) of Japan and by a Sasagawa Scientific Research Grant from The Japan Science Society.

SUPPLEMENTARY MATERIALS

Supplementary data associated with this article can be found in the online version at http://www.aaqr.org.

REFERENCES

Arakaki, T., Kuroki, Y., Okada, K., Nakama, Y., Ikota, H., Kinjo, M., Higuchi, T., Uehara, M. and Tanahara, A. (2006). Chemical Composition and Photochemical Formation of Hydroxyl Radicals in Aqueous Extracts of Aerosol Particles Collected in Okinawa, Japan. *Atmos. Environ.* 40: 4764–4774, doi: 10.1016/j.atmosenv.2006.04.035.

Bhanuprasad, S.G., Venkataraman, C. and Bhushan, M. (2008). Positive Matrix Factorization and Trajectory Modelling for Source Identification: A New Look at Indian Ocean Experiment Ship Observations. *Atmos. Environ.* 42: 4836–4852, doi:10.1016/j.atmosenv.2008.02.041.

Bond, C.T., Doherty, J.S., Fahey, W.D., Forster, M.P., Berntsen, T., DeAngelo, J.B., Flanner, G.M., Ghan, S., Kärcher, B., Koch, D., Kinne, S., Kondo, Y., Quinn, K.P., Sarofim, C.M., Schultz, G.M., Schulz, M., Venkataraman, C., Zhang, H., Zhang, S., Bellouin, N., Guttikunda, K.S., Hopke, K.P., Jacobson, Z.M., Kaiser, W.J., Klimont, Z., Lohmann, U., Schwarz, P.J., Shindell, D., Storelvmo, T., Warren, G.S., Zender, S.C. (2013). Bounding the Role of Black Carbon in the Climate System: A Scientific Assessment. *J. Geophys. Res.* 118: 5380–5552, doi: 10.1002/jgrd.5017.

Cherian, R., Venkataraman, C., Kumar, A., Sarin, M.M., Sudheer, K.A. and Ramachandran, S. (2010). Source Identification of Aerosols Influencing Atmospheric Extinction: Integrating PMF and PSCF with Emission Inventories and Satellite Observations. *J. Geophys. Res.* 115: D22212, doi: 10.1029/2009/JD012975.

Chow, J.C., Watson, G.J., Crow, D., Lowenthal, H.D. and Merrifield, T. (2001). Comparison of IMPROVE and NIOSH Carbon Measurements. *Aerosol Sci. Technol.* 34: 23–34, doi: 10.1080/02786820119073.

Draxler, R.R. and Rolph D.G. (2003). Hybrid Single-Particle

Lagrangian Integrated Trajectory (HYSPLIT) Model Access via the NOAA Website http://www.arl.noaa.gov/ready/hysplit4.html, NOAA Air Resources Laboratory, Silver Spring, MD.

Feng, J., Hu, M., Chan, K.C., Lau, S.P., Fang, M., He, L. and Tang, X. (2006). A Comparative Study of the Organic Matter in $PM_{2.5}$ from Three Chinese Megacities in Three Different Climatic Zones. *Atmos. Environ.* 40: 3983–3994, doi: 10.1016/j.atmosenv.2006.02.017.

Flowers B.A., Dubey, K.M., Mazzoleni, C., Stone, A.E., Schauer, J.J., Kim, W.S. and Yoon, C.S. (2010). Optical-chemical-microphysical Relationships and Closure Studies for Mixed Carbonaceous Aerosols Observed at Jeju Island; 3-laser Photoacoustic Spectrometer, Particle Sizing, and Filter Analysis. *Atmos. Chem. Phys.* 10: 10387–10398, doi: 10.5194/acp-10-10387-2010.

Gao, Y., Nelson, D.E., Field, P.M., Ding, Q., Li, H., Sherrell, R.M., Gigliotti, C.L., Ryda, V., Glenn, T.R. and Eisenreich, S.J. (2002). Characterization of Atmospheric Trace Elements on $PM_{2.5}$ Particulate Matter over the New York–New Jersey Harbor Estuary. *Atmos. Environ.* 36: 1077–1086, doi: 10.1016/S1352-2310(01) 00381-8.

Gelencser, A. (2004). *Carbonaceous Aerosol*. Springer, Dordrecht, Netherlands.

Green, D., Alexander, J., Fuller, G., Quincey, P., and Butterfield, D. (2007). Marylebone Road Aethalometer Trial Report. Available through the Defra website www.airquality.co.uk., UK-AIR: Air Information Resource.

Gustafsson, Ö., Kruså, M., Zencak, Z., Sheesley, R.J., Granat, L., Engström, E., Praveen, P.S., Rao, P.S.P., Leck, C. and Rodhe, H. (2009). Brown Clouds over South Asia, Biomass or Fossil Fuel Combustion? *Science* 323: 495–498.

Han, S., Kondo, Y., Oshima, N., Takegawa, N., Miyazaki, Y., Hu, M., Lin, P., Deng, Z., Zhao, Y., Sugimoto, N. and Wu, Y. (2009). Temporal Variations of Elemental Carbon in Beijing. *J. Geophys. Res.*114: D23202, doi: 10.1029/2009JD012027.

Handa, D., Nakajima, H., Arakaki, T., Kumata, H., Shibata, Y. and Uchida, M. (2010). Radiocarbon Analysis of BC and OC in PM_{10} Aerosols at Cape Hedo, Okinawa, Japan, during Long-range Transport Events from East Asian Countries. *Nucl. Instrum. Methods Phys. Res., Sect. B* 268: 1125–1128, doi:10.1016/j.nimb.2009.10.115.

Hansen, S.J., Sato, M., Ruedy, R., Nazarenko, L., Lacis, A., Schmidt, G.A., Russell, G., Aleinov, I., Bauer, M., Bauer, S., Bell, N., Cairns, B., Canuto, V., Chandler, M., Cheng, Y., Del Genio, A., Faluvegi, G., Fleming, E., Friend, A., Hall, T., Jackman, C., Kelley, M., Kiang, N., Koch, D., Lean, J., Lerner, J., Lo, K., Menon, S., Miller, R., Minnis, P., Novakov, T., Oinas, V., Perlwitz, Ja., Perlwitz, Ju., Rind, D., Romanou, A., Shindell, D., Stone, P., Sun, S., Tausnev, N., Thresher, D., Wielicki, B., Wong, T., Yao, M. and Zhang, S. (2005). Efficacy of Climate Forcings. *J. Geophys. Res*. 110: D 18104, doi: 10.1029/2005JD005776.

Hasegawa, S. (2014). Estimation of Influence of Artifact on Carbonaceous Aerosol Measurement. Proceedings of 2014 International Aerosol Conference, p. 16-094.

Hatakeyama, S., Hanaoka, S., Ikeda, K., Watanabe, I., Arakaki, T., Sadanaga, Y., Bandow, H., Kato, S., Kajii, Y., Sato, K., Shimizu, A. and Takami, A. (2011). Aerial Observation of Aerosols Transported from East Asia Chemical Composition of Aerosols and Layered Structure of an Air Mass over the East China Sea. *Aerosol Air Qual. Res.* 11: 497–507, doi: 10.4209/aaqr.2011.06.0076.

Hatakeyama, S., Ikeda, K., Hanaoka, S., Watanabe, I., Arakaki, T., Bandow, H., Sadanaga, Y., Kato, S., Kajii, Y., Zhang, D., Okuyama, K., Ogi, T., Fujimoto, T., Seto, T., Shimizu, A., Sugimoto, N. and Takami, A. (2014). Aerial Observations of Air Masses Transported from East Asia to the Western Pacific: Vertical Structure of Polluted Air Masses. *Atmos. Environ.* 97: 456–461.

Hatakeyama, S., Murano, K., Mukai, H., Sakamaki, F., Bandow, H. and Komazaki, Y. (2001). Transport of Atmospheric Pollutants from East Asia. *Water Air Soil Pollut.* 130: 373–378.

Hatakeyama, S., Takami, A., Miyoshi, T. and Wang, W. (2006). Relationship among Major Ionic Species in Aerosols Transported from China via the East China Sea to Okinawa. *Earozoru Kenkyu (J. Aerosol Res.)* 21: 147–152 (in Japanese).

Hidemori, T., Nakayama, T., Matsumi, Y., Kinugawa, T., Yabushita, A., Ohashi, M., Miyoshi, T., Irei, S., Takami, A., Kaneyasu, N., Yoshino, A., Suzuki, R., Yumoto, Y. and Hatakeyama, S. (2014). Characteristics of Atmospheric Aerosols Containing Heavy Metals Measured on Fukue Island, Japan. *Atmos. Environ.* 97: 447–455, doi: 10.1016/j.atmosenv.2014.05.008.

Hopke, P.K., Barrie, A.L., Li, M.S., Cheng, D.M., Li, C. and Xie, Y. (1995). Possible Sources and Preferred Pathways for Biogenic and Non-sea-salt Sulfur for the High Arctic, *J. Geophys. Res.* 100: D8

Jacobson, M. Z. (2010). Short-term Effects of Controlling Fossil-fuel Soot, Biofuel Soot and Gases, and Methane on Climate, Arctic Ice, and Air Pollution Health. *J. Geophys. Res.* 115: D14209, doi: 10.1029/2009JD013795.

Jeong, J.I., Park , J.R., Woo, H.J., Han, J.Y. and Yi, M.S. (2011). Source Contributions to Carbonaceous Aerosol Concentrations in Korea. *Atmos. Environ.* 45: 1116–1125.

Kanaya, Y., Komazaki, Y., Pochanart, Y., Liu, Y., Akimoto, H., Gao, J., Wang, T. and Wang, Z. (2008). Mass Concentrations of Black Carbon Measured by Four Instruments in the Middle of Central East China in June 2006. *Atmos. Chem. Phys.* 8: 7637–7649, doi: 10.5194/acp-8-7637-2008.

Kaneyasu, N. (2010). Development of $PM_{2.5}$ Impactor for the Conventional High-volume Air Sampler. *J. Japan Soc. Atmos. Environ.* 45: 171–174 (in Japanese).

Kim, E. and Hopke, P.K. (2004). Improving Source Identification of fine Particles in a Rural Northeastern US area Utilizing Temperature Resolved Carbon Fractions, *J. Geophys. Res.* 109: D09204, doi: 10.1029/2003JD004199.

Kim, E., Hopke, P.K. and Edgerton, E.S. (2004). Improving Source Identification of Atlanta Aerosol Using Temperature Resolved Carbon Fractions in Positive Matrix Factorization. *Atmos. Environ*. 38: 3349–3362,

doi: 10.1016/j.atmosenv.2004.03.012.

Kitayama, K., Murao, N. and Hara, H. (2010). PMF Analysis of Impacts of SO_2 from Miyakejima and Asian Continent on Precipitation Sulfate in Japan. *Atmos. Environ*. 44: 95–105.

Koch, D., Balkanski, Y., Bauer, E.S., Easter, C.R., Ferrachat, S., Ghan, J.S., Hoose, C., Iversen, T., Kirkevåg, A., Kristjansson, E.J., Liu, X., Lohmann, U., Menon, S., Quaas, J., Schulz, M., Seland, Ø., Takemura, T. and Yan, N. (2011). Soot Microphysical Effects on Liquid Clouds, a Multi-model Investigation. *Atmos. Chem. Phys.* 11: 1051–1064, doi: 10.5194/acp-11-1051-2011.

Kondo, Y., Komazaki, Y., Miyazaki, Y., Moteki, N., Takegawa, N., Kodama, D., Deguchi, S., Nogami, M., Fukuda, M., Miyakawa, T., Morino, Y., Koike, M., Sakurai, H. and Ehara, K. (2006).Temporal Variations of Elemental Carbon in Tokyo. *J. Geophys. Res.* 111: D12205, doi: 10.1029/2005JD006257.

Laskin, A., Wietsma, W.T., Krueger, J. B. and Grassian, H.V. (2005). Heterogeneous Chemistry of Individual Mineral Dust Particles with Nitric Acid: A Combined CCSEM/EDX, ESEM, and ICP-MS study. *J. Geophys. Res.* 110: D10208, doi: 10.1029/2004JD005206.

Lee, M., Song, M., Moon, K.J., Han, J.S., Lee, G. and Kim, R.K. (2007). Origins and Chemical Characteristics of Fine Aerosols during the Northeastern Asia Regional Experiment (Atmospheric Brown Cloud–East Asia Regional Experiment 2005). *J. Geophys. Res.* 112: D22S29, doi: 10.1029/2006JD008210.

Lei, Y., Zhang, Q., He, B.K. and Streets, G.D. (2011). Primary Anthropogenic Aerosol Emission Trends for China, 1990–2005. *Atmos. Chem. Phys.* 11: 931–954, doi: 10.5194/acp-11-931-2011.

Lin, J.J. and Tai, H.S. (2001). Concentrations and Distributions of Carbonaceous Species in Ambient Particles in Kaohsiung City, Taiwan. *Atmos. Environ.* 35: 2627–2636, doi: 10.1016/S1352-2310(00)00444-1.

Lin, M.Y., Oki, T., Holloway, T., Streets, G.D., Bengtsson, M. and Kanae, S. (2008). Long-range Transport of Acidifying Substances in East Asia – Part I - Model Evaluation and Sensitivity Studies. *Atmos. Environ.* 42: 5939–5955, doi: 10.1016/j.atmosenv.2008.04.008.

Matsumoto, K., Uematsu, M., Hayano, T., Yoshioka, K., Tanimoto, H. and Iida, T. (2003). Simultaneous Measurements of Particulate Elemental Carbon on the Ground Observation Network over the Western North Pacific during the ACE-Asia Campaign. *J. Geophys. Res.* 108: 8635, doi: 10.1029/2002JD002744.

Mehta, B., Venkataraman, C., Bhushan, M. and Tripathi, N.S. (2009). Identification of Sources Affecting Fog Formation Using Receptor Modeling Approaches and Inventory Estimates of Sectoral Emissions. *Atmos. Environ.* 43: 1288–1295, doi: 10.1016/j.atmosenv.2008.11.041.

Miyazaki, Y., Kondo, Y., Han, S., Koike, M., Kodama, D., Komazaki, Y., Tanimoto, Y. and Matsueda, H. (2007). Chemical Characteristics of Water-soluble Organic Carbon in the Asian Outflow. *J. Geophys. Res.* 112: D22S30, doi: 10.1029/2007JD009116.

Miyazaki, Y., Kondo, Y., Takegawa, N., Komazaki, Y., Fukuda, M., Kawamura, K., Mochida, M., Okuzawa, K., and Weber, J.R. (2006). Time-resolved Measurements of Water-soluble Organic Carbon in Tokyo. *J. Geophys. Res.* 111: 1–12, doi: 10.1029/2006JD007125.

Moteki, N., Kondo, Y., Miyazaki, Y., Takegawa, N., Komazawa, Y., Kurata, G., Shirai, T., Blake, R. D., Miyakawa, T. and Koike, M. (2007). Evolution of Mixing State of Black Carbon Particles: Aircraft Measurements over the Western Pacific in March 2004. *Geophys. Res. Lett.* 34: L11803, doi: 10.1029/2006GL028943.

Nakajima, T., Yoon, C.S., Ramanathan, V., Shi, Y.G., Takemura, T., Higurashi, A., Takamura, T., Aoki, K., Sohn, J.B., Kim, W.S., Tsuruta, H., Sugimoto, N., Shimizu, A., Tanimoto, H., Sawa, Y., Lin, H.N., Lee, T.C., Goto, D. and Schutgens, N. (2007). Overview of the Atmospheric Brown Cloud East Asian Regional Experiment 2005 and a Study of the Aerosol Direct Radiative Forcing in East Asia. *J. Geophys. Res.* 112: D24S91, doi: 10.1029/2007JD009009.

Norris, G., Vedantham, R., Wade, K., Brown, S., Prouty, J., Foley, C. and Martin, L. (2008). EPA Positive Matrix Factorization (PMF) 3.0 Fundamentals & User Guide. Environmental Protection Agency (EPA). 600/R-08/108.

Novakov, T., Menon, S., Kirchstetter, W.T., Koch, D. and Hansen, J.E. (2005). Aerosol Organic Carbon to Black Carbon Ratios: Analysis of Published Data and Implications for Climate Forcing. *J. Geophys. Res.* 110: D21205, doi: 10.1029/2005JD005977.

Ohara, T., Akimoto, H., Kurokawa, J., Horii, N., Yamaji, K., Yan, X. and Hayasaka, T. (2007). An Asian Emission Inventory of Anthropogenic Emission Sources for the Period 1980–2020. *Atmos. Chem. Phys.* 7: 4419–4444, doi: 10.5194/acp-7-4419-2007.

Okuda, T., Tenmoku, M., Kato, J., Mori, J., Sato, T., Yokouchi, R. and Tanaka, S. (2006). Long-term Observation of Trace Metal Concentration in Aerosols at a Remote Island, Rishiri, Japan by Using Inductively Coupled Plasma Mass Spectrometry Equipped with Laser Ablation. *Water Air Soil Pollut.* 174: 3–17, doi: 10.1007/s11270-005-9000-2.

Oshima, N., Koike, M., Zhang, Y., Kondo, Y., Moteki, N., Takegawa, N. and Miyazaki, Y. (2009). Aging of Black Carbon in Outflow from Anthropogenic Sources Using a Mixing State Resolved Model: Model Development and Evaluation. *J. Geophys. Res.* 114: D06210, doi: 10.1029/2008JD010680.

Oshima, N., Kondo, T., Moteki, N., Takegawa, N., Koike, M., Kita, K., Matsui, H., Kajino, M., Nakamura, H., Jung, S.J. and Kim, J.Y. (2012). Wet Removal of Black Carbon in Asian Outflow: Aerosol Radiative Forcing in East Asia (A-FORCE) Aircraft Campaign. *J. Geophys. Res.* 117: D03204, doi: 10.1029/2011JD016552.

Paatero, P. and Tapper, U. (1994). Positive Matrix Factorization: A Non-negative Factor Model with Optimal Utilization of Error Estimates of Data Values. *Environmetrics* 5: 111–126.

Pekney, N.J., Davidson, C.I., Zhou, L. and Hopke, P.K. (2006). Application of PSCF and CPF to PMF-modeled

Sources of $PM_{2.5}$ in Pittsburgh. *Aerosol Sci. Technol.* 40: 952–961, doi: 10.1080/02786820500543324.

Quincey, P., Butterfield, D., Green, D., Coyle, M. and Cape, N.J. (2009). An Evaluation of Measurement Methods for Organic, Elemental and Black Carbon in Ambient Air Monitoring Sites. *Atmos. Environ.* 43: 5085–5091, doi: 10.1016/j.atmosenv.2009.06.041.

Ramana, M.V., Ramanathan, V., Feng, Y., Yoon, C.S., Kim, W.S., Carmichael, R. G. and Schauer, J.J. (2010). Warming Influenced by the Ratio of Black Carbon to Sulphate and the Black-carbon Source. *Nat. Geosci.* 3: 542–545, doi: 10.1038/ngeo918.

Ramanathan, V., Crutzen, J.P., Mitra, P.A. and Sikka, D. (2002). The Indian Ocean Experiment and the Asian Brown Cloud. *Curr. Sci.* 83: 947– 955.

Ramanathan, V., Li, F., Ramana, V.M., Praveen, S.P., Kim, D., Corrigan, E.C., Nguyen, H., Stone, A.E., Schauer, J.J., Carmichael, R.G., Adhikary, B. and Yoon, C.S. (2007). Atmospheric Brown Clouds: Hemispherical and Regional Variations in Long-range Transport, Absorption and Radiative Forcing. *J. Geophys. Res.* 112: D22S21, doi: 10.1029/2006JD008124.

Richter, A., Eyring, V., Burrows, P.J., Bovensmann, H., Lauer, A., Sierk, B. and Crutzen, J.P. (2004). Satellite Measurements of NO_2 from International Shipping Emissions. *Geophys. Res. Lett.* 31: L23110, doi: 10.1029/2004GL020822.

Shimada, K., Takami, A., Kato, S., Yoshizumi, K. and Hatakeyama, S. (2011). Variation of Carbonaceous Aerosol in Polluted Air Mass Transported from East Asia and Evaluation of Their Source Origin. *J. Japan Soc. Atmos. Environ.* 25: 1–11 (in Japanese).

Stone, E.A., Lough, C.G., Schauer, J.J., Praveen, S.P., Corrigan, E.C. and Ramanathan, V. (2007). Understanding the Origin of Black Carbon in the Atmospheric Brown Cloud over the Indian Ocean, *J. Geophys. Res.* 112: D22S23, doi: 10.1029/2006JD008118.

Takami, A., Miyoshi, T., Shimono, A., Kaneyasu, N., Kato, S., Kajii, Y. and Hatakeyama, S. (2007). Transport of Anthropogenic Aerosols from Asia and Subsequent Chemical Transformation, *J. Geophys. Res.* 112: D22S31, doi: 10.1029/2006JD008120.

Takiguchi, Y., Takami, A., Sadanaga, Y., Lun, X., Shimizu, A., Matsui, I., Sugimoto, N., Wang, W., Bandow, H. and Hatakeyama, S. (2008). Transport and Transformation of Total Reactive Nitrogen over the East China Sea. *J. Geophys. Res.,* 113: D10306, doi: 10.1029/2007JD009462.

UNEP and WMO (2011). *I*ntegrated Assessment of Black Carbon and Tropospheric Ozone: Summary for Decision Makers. Available through UNEP Website http://www.rrcap.unep.org/abc/impact/.

Uno, I., Jang, S.E., Shimohara, T., Oishi, O., Utsunomiya, A., Hatakeyama, S., Murano, K., Tang, X. and Kim, P. Y. (2000). Wintertime Intermittent Transboundary air Pollution over East Asia Simulated by a Long-range Transport Model. *Global Environ. Res.* 4: 3–12.

Xu, B., Cao, J., Hansen, J., Yao, T., Joswia, R. D., Wang, N., Wu, G., Wang, M., Zhao, H., Yang, W., Liu, X. and He, J. (2009). Black Soot and the Survival of Tibetan Glaciers. *Proc. Nat. Acad. Sci. U.S.A.* 106: 22114–22118, doi: 10.1073/pnas.0910444106.

Xu, M., Yan, R., Zheng, C., Qiao, Y., Han, J. and Sheng, C. (2003). Status of Trace Element Emission in Coal Combustion Process: A Review. *Fuel Proc. Technol.* 85: 215–237, doi: 10.1016/S0378-3820(03)00174-7.

Yamaji, K., Li, J., Uno, I., Kanaya, Y., Komazaki, Y., Pochanart, P., Liu, Y., Takigawa, M., Ohara, T., Yan, X., Wang, Z. and Akimoto, H. (2009). Impact of Open Crop Residual Burning on Air Quality over Central Eastern China during the Mount Tai Experiment 2006 (MTX2006). *Atmos. Chem. Phys.* 9: 22103–22141, doi: 10.5194/acpd-9-22103-2009.

Zhang, Q., Streets, G.D., Carmichael, R.G., He, B.K., Huo, H., Kannari, A., Klimont, Z., Park, S.I., Reddy, S., Fu, S.J., Chen, D., Duan, L., Lei, Y., Wang, T.L. and Yao, L.Z. (2009). Asian Emissions in 2006 for the NASA INTEX-B Mission. *Atmos. Chem. Phys.* 9: 5131–5153, doi: 10.5194/acp-9-5131-2009.

Zhang, X.Y., Wang, Q.Y., Zhang, C.X., Guo, W. and Gong, L.S. (2008). Carbonaceous Aerosol Composition over Various Regions of China during 2006. *J. Geophys. Res.* 113: D14111, doi: 10.1029/2007JD009525.

Zhu, X.Y., Duan, L., Tang, G.G., Hao, J.M. and Dong, G.X. (2004). Estimation of Atmospheric Emissions of Base Cations in China. *J. Tsinghua Univ. Sci. Technol.* 44: 1176–1179 (in Chinese).

Received for review, October 21, 2014
Revised, December 29, 2014
Accepted, December 30, 2014

Supporting Information for:

Mode and place of origin of carbonaceous aerosols transported from East Asia to Cape Hedo, Okinawa Japan

Kojiro Shimada[1,2*], Masamichi Shimada[1], Akinori Takami[3], Shuichi Hasegawa[4], Akihiro Fushimi[3], Takemitsu Arakaki[5], Izumi Wanatabe[1] Shiro Hatakeyama[1]

[1] Graduate School of Agriculture, Tokyo University of Agriculture and Technology, 3-5-8 Saiwaicho, Fuchu, Tokyo 183-8509, Japan

[2] Tokyo Metropolitan Research Institute for Environmental Protection, 1-7-5 Shinsuna, Kouto, Tokyo 136-0075, Japan

[3] National Institute for Environmental Studies, 16-2 Onogawa, Tsukuba, Ibaraki 305-8506, Japan

[4] Center for Environmental Science in Saitama, 914 Kamitanadare, Kazo, Saitama 347-0115, Japan

[5] University of the Ryukyus, 1 Senbaru, Nishihara-cho, Okinawa 903-0213, Japan

The Supporting Information contains 12 Figures and 1 Table.

Supplementary Figures and Table: Choosing the optimal number of factors for the model is challenging. To determine the optimal number of factors, it is necessary first to determine the minimum Q values for different numbers of factors. Different Q functions can be defined that $Q_{(true)}$ is the goodness of fit parameter calculated including all points. $Q_{(robust)}$ is the goodness of fit parameter calculated excluding points not fit by the model, defined as samples for which the uncertainty scaled residual is greater than 4. We basically followed the method presented by Norris *et al.* (2008), although several different methods have been proposed (Bhanuprasad *et al.*, 2008; Kitayama *et al.*, 2010; Cherian *et al.*, 2010; Norris *et al.*, 2008). In this study, we first investigated minimum Q values (Fig. S1(a)).

Fig. S1(a) shows that the slope of the relationship between the minimum Q value and the number of factors began to level off at five factors. The reduction in Q with the increase in the number of factors and the agreement of estimated Q with its theoretical value, Q_{theo}, were used to identify possible optimal solutions. However, with this method, the results for 4, 5, and 6 factors are similar.

To identify the minimum number of factors needed for a well-constrained solution, we examined the maximum individual column mean (IM) and the maximum individual column standard deviation (IS) (Fig. S1(b)). These scaled residual matrix values dropped sharply for solutions with 5 or more factors. Therefore, we adopted 5 as the optimal number of factors. In, We then evaluated the resultant PMF calculations (Figs. S2 and S3 and Table S1). We removed several chemical components with poor correlation factors (R^2) because the model results for these chemical components seemed unreasonable. In these cases, the number of data were insufficient, or the uncertainties were high. Table S1 also shows the number of missing values and of values below the detection limit. The PMF model does not allow values below the detection limit or missing values to be implemented. Instead, they are replaced by "virtual" values having larger uncertainties in order to lower their influence on the PMF modeling result (Polissar *et al.*, 1998; Reff *et al.*, 2007). Some metallic components had values that were below the detection limit in this study; these values were replaced with half the detection limit value, and their estimated errors were evaluated as 5/6 of the detection limit (Norris *et al.*, 2008). In the case of missing data, they are applied geometric or arithmetic values (Bhanuprasad *et al.*, 2008; Cherian *et al.*, 2010). In this study, missing values were replaced with the median value for that species, and the uncertainty was set at 4 times the species-specific median, as suggested by Norris *et al*. (2008). Some OC and EC measurement data were defective in both summer (18 and 20

July) and winter (10, 11, and 13 January). These data, because they were only "virtual," were excluded from the analysis results presented in Fig. 6. The measurement uncertainties (i.e., the method detection limits) were determined following the procedure of Norris *et al.* (2008). In this study, these values were low. Bhanuprasad *et al.* (2008) used one standard deviation of the blank measurement values as the MDL data set.

To evaluate the uncertainties, we examined the interquartile ranges of the contributions of the 5 factor contributions and the concentrations of key species (Fig. S2 and S3). These ranges were around 20% or less. Bhanuprasad *et al.* (2008), Mehta *et al.* (2009), and Cherian *et al.* (2010) reported that the estimated uncertainty for the contribution of each factor was < ~15%, and Norris et al. (2008) evaluated the estimated uncertainty to be around 30%.

REFERENCES

Bhanuprasad, S. G., Venkataraman, C. and Bhushan, M. (2008). Positive matrix factorization and trajectory modelling for source identification: A new look at Indian Ocean Experiment ship observations. *Atmos. Environ*. 42: 4836–4852, doi:10.1016/j.atmosenv.2008.02.041.

Cherian, R., Venkataraman, C., Kumar, A., Sarin, M. M., Sudheer, K. A. and Ramachandran, S. (2010). Source identification of aerosols influencing atmospheric extinction: Integrating PMF and PSCF with emission inventories and satellite observations. *J. Geophys. Res.* 115: D22212, doi:10.1029/2009/JD012975.

Mehta, B., Venkataraman, C., Bhushan, M. and Tripathi, N. S. (2009). Identification of sources affecting fog formation using receptor modeling approaches and inventory estimates of sectoral emissions. *Atmos. Environ.* 43: 1288–1295, doi:10.1016/j.atmosenv.2008.11.041.

Norris, G., Vedantham, R., Wade, K., Brown, S., Prouty, J., Foley, C. and Martin, L. (2008). EPA Positive Matrix Factorization (PMF) 3.0 Fundamentals & User Guide. E*nvironmental Protection Agency (EPA)*. 600/R-08/108.

Kitayama, K., Murao, N. and Hara, H. (2010). PMF analysis of impacts of SO_2 from Miyakejima and Asian Continent on precipitation sulfate in Japan. *Atmos.*

Environ. 44: 95-105.

Polissar, A., Hopke, P., Paatero, P. (1998). Atmospheric aerosol over Alaska - 2. Elemental composition and sources, *J. Geophys. Res.*, 103(D15), 19045–19057, doi:10.1029/98JD01212.

Reff, A., Eberly, S. I. and Bhave, P. V. (2007). Receptor modeling of ambient particulate matter data using positive matrix factorization: review of existing methods, *J. Air. Waste. Manage. Assoc.,* 57(2), 146, 2007.

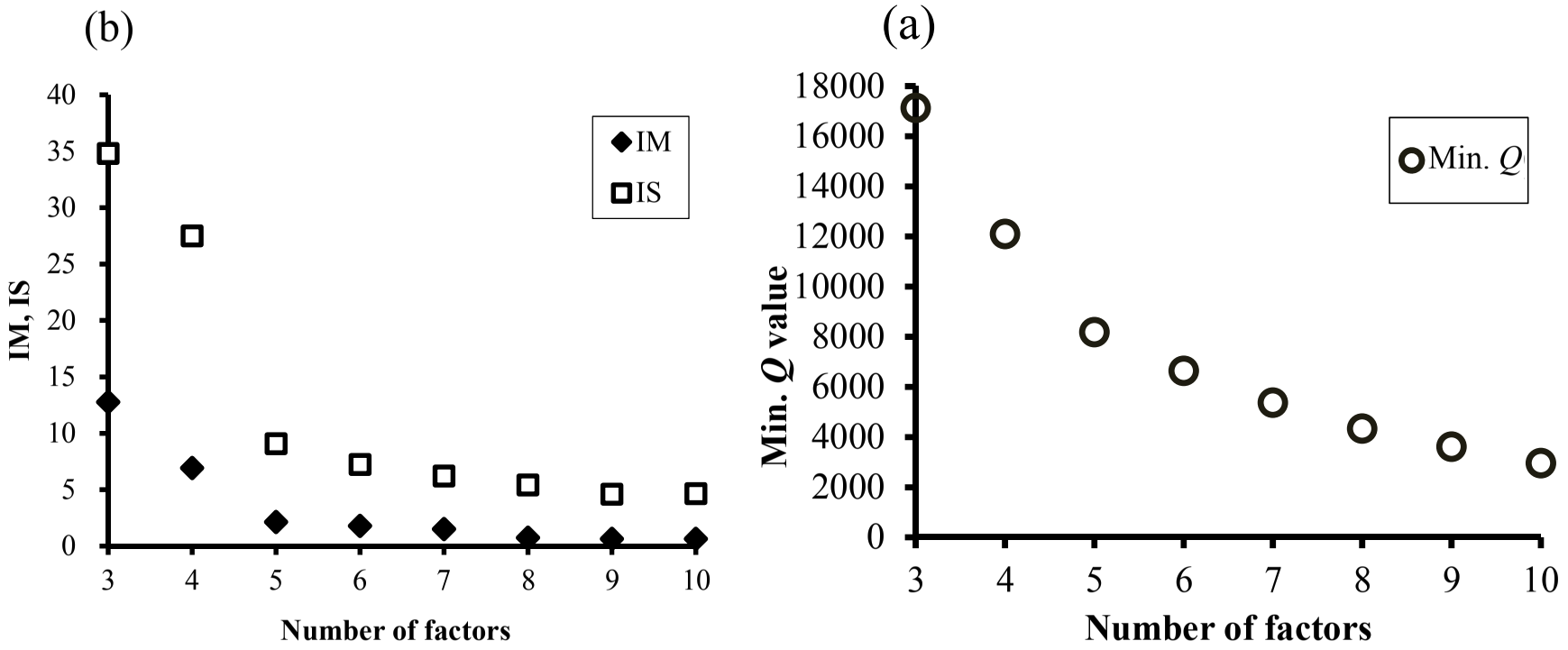

Fig. S1. Determination of the minimum number of factors needed for a well-constrained solution based on (a) minimum *Q* and (b) IM and IS values.

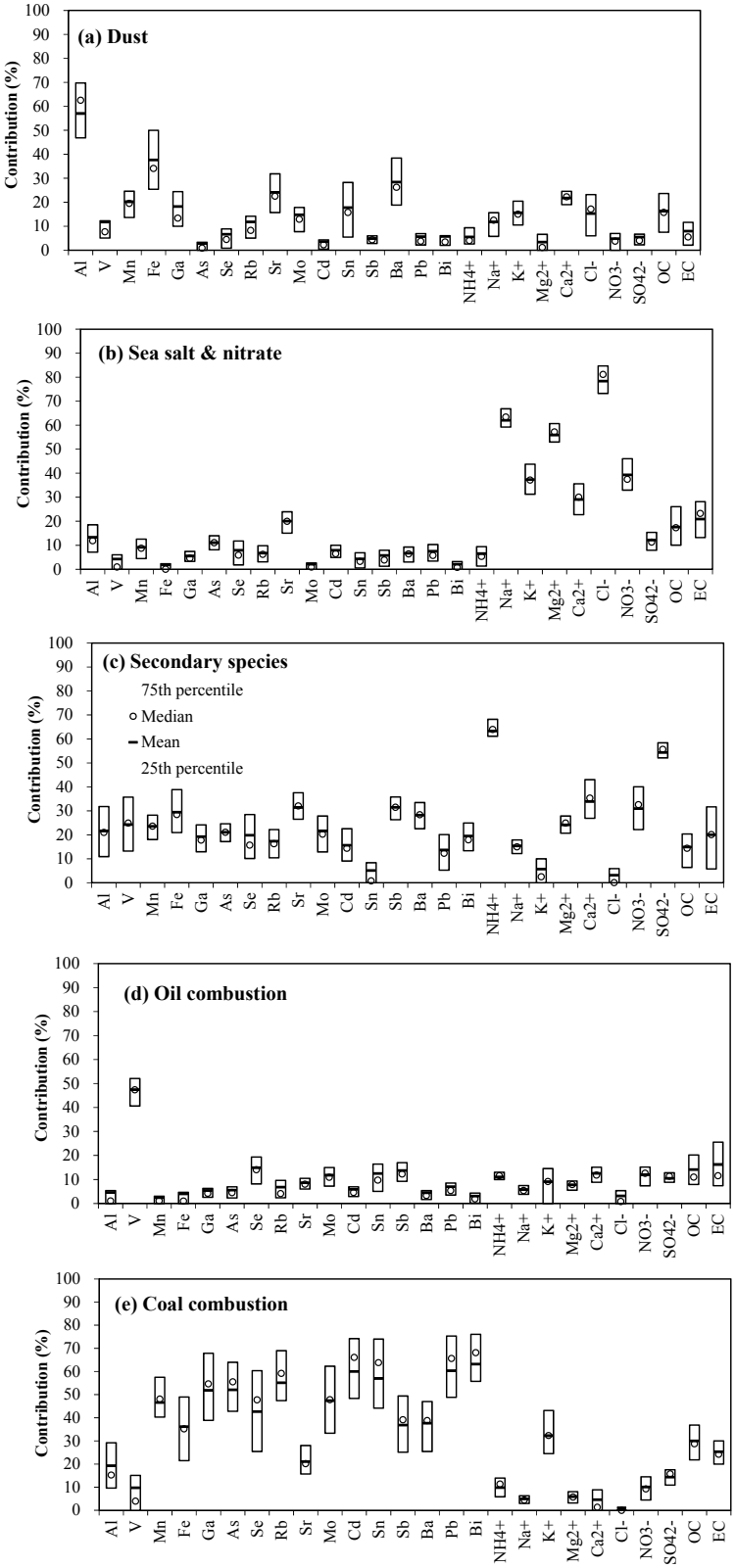

Fig. S2. The profiles obtained by bootstrapping of the relative contributions of (a) dust, (b) sea salt and nitrate, (c) secondary species, (d) oil combustion, and (e) coal combustion.

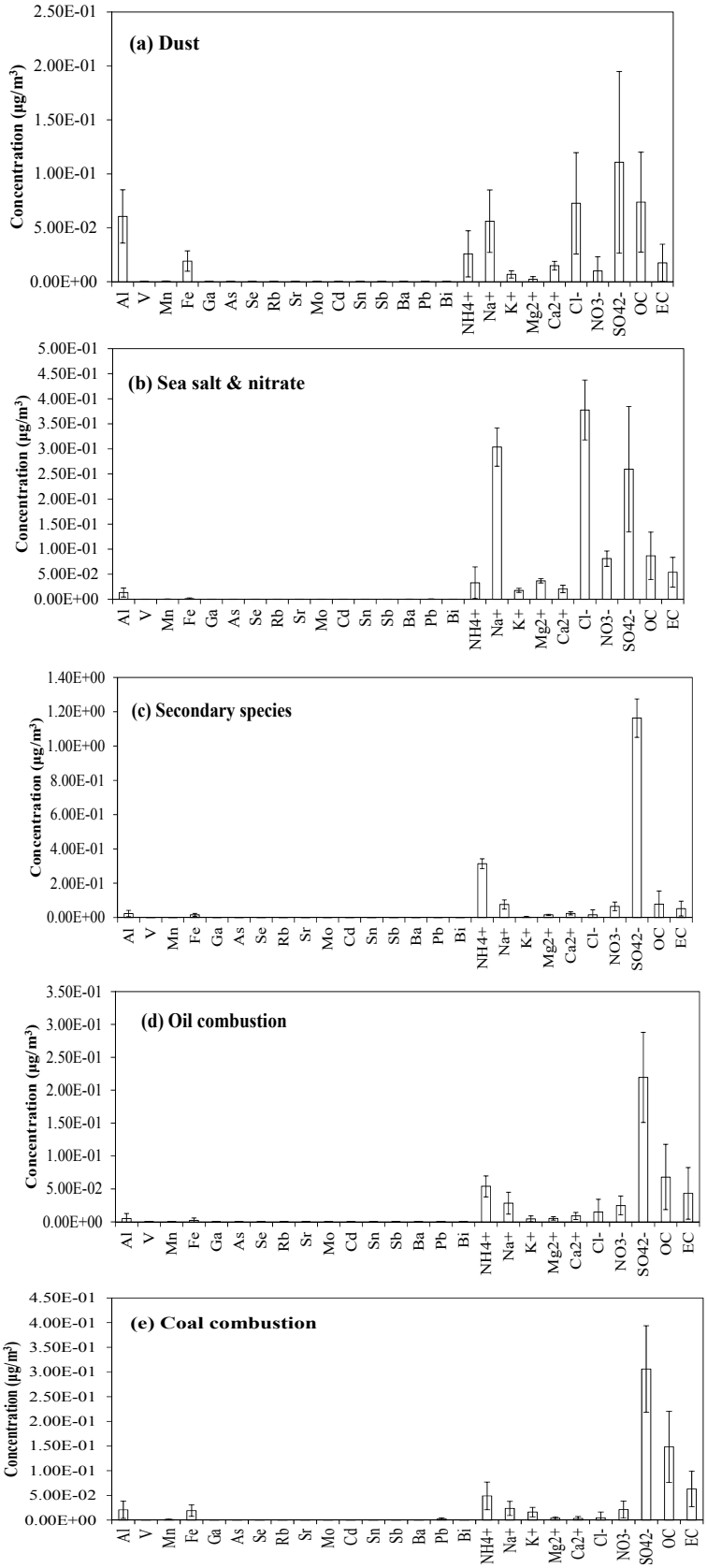

Fig. S3. The profiles obtained by bootstrapping of the absolute contributions (μg/m^3) of (a) dust, (b) sea salt and nitrate, (c) secondary species, (d) oil combustion, and (e) coal combustion. Error bars mean one standard deviation

Table S1. Summary of aerosol chemical measurements made throughout 2010 at CHAAMS

Spceies	Slope and R^2 (predicted versus observed)	No. of values below the detection limit	No. of missing values	Number of samples
Al	0.99 (R^2 = 0.99)	0	0	45
V	0.99 (R^2 = 0.99)	0	0	45
Mn	0.87 (R^2 = 0.93)	0	0	45
Fe	0.78 (R^2 = 0.83)	11.1	0	45
Ga	0.96 (R^2 = 0.94)	0	0	45
As	0.92 (R^2 = 0.94)	0	0	45
Se	0.76 (R^2 = 0.7)	11.1	0	45
Rb	0.88 (R^2 = 0.86)	0	0	45
Sr	0.78 (R^2 = 0.78)	0	0	45
Mo	0.57 (R^2 = 0.78)	0	0	45
Cd	0.97 (R^2 = 0.96)	11.1	0	45
Sn	0.78 (R^2 = 0.78)	0	0	45
Sb	0.89 (R^2 = 0.85)	0	0	45
Ba	0.87 (R^2 = 0.92)	0	0	45
Pb	0.96 (R^2 = 0.95)	0	0	45
Bi	0.96 (R^2 = 0.96)	0	0	45
NH_4^+	0.99 (R^2 = 0.99)	0	0	45
Na+	0.99 (R^2 = 0.99)	0	0	45
K^+	0.51 (R^2 = 0.78)	0	0	45
Mg^{2+}	0.89 (R^2 = 0.93)	0	0	45
Ca^{2+}	0.89 (R^2 = 0.88)	8.8	0	45
Cl^-	1.0 (R^2 = 0.96)	0	0	45
NO_3^-	0.60 (R^2 = 078)	0	0	45
SO_4^{2-}	1.0 (R^2 = 0.97)	0	0	45
OC	0.87 (R^2 = 0.87)	0	11.1	40
EC	0.90 (R^2 = 0.90)	0	11.1	40